Mapping Intrapatient Response Heterogeneity and Lesion-specific Relapse Dynamics in Metastatic Colorectal Cancer

Jiawei Zhou
University of North Carolina at Chapel Hill
Amber Cipriani
University of North Carolina at Chapel Hill https://orcid.org/0000-0003-3596-0581
Yutong Liu
University of North Carolina at Chapel Hill
Gang Fang
University of North Carolina at Chapel Hill
Quefeng Li
University of North Carolina at Chapel Hill
Yanguang Cao (yanguang@unc.edu)
University of North Carolina at Chapel Hill https://orcid.org/0000-0002-3974-9073

Article

Keywords:

Posted Date: March 28th, 2022

DOI: https://doi.org/10.21203/rs.3.rs-1447896/v1

Mapping Intrapatient Response Heterogeneity and Lesion-specific Relapse Dynamics in Metastatic Colorectal Cancer

Jiawei Zhou[1], Amber Cipriani[1,2], Yutong Liu[3], Gang Fang[4], Quefeng Li[3], Yanguang Cao[1,5*]

[1]Division of Pharmacotherapy and Experimental Therapeutics, School of Pharmacy, University of North Carolina at Chapel Hill, NC 27599, USA; [2]UNC Health Medical Center, Department of Pharmacy, Chapel Hill, NC 27514; [3]School of Public Health, University of North Carolina at Chapel Hill, NC 27599, USA; [4]Division of Pharmaceutical Outcomes and Policy, School of Pharmacy, University of North Carolina at Chapel Hill, NC 27599, USA; [5]Lineberger Comprehensive Cancer Center, School of Medicine, University of North Carolina at Chapel Hill, Chapel Hill, NC 27599, USA

Corresponding author:

Yanguang Cao, Ph.D.

Division of Pharmacotherapy and Experimental Therapeutics, UNC School of Pharmacy

2318 Kerr Hall, UNC Eshelman School of Pharmacy

Chapel Hill, NC 27599-7569

E-mail: yanguang@unc.edu

Phone: +1-919-966-4040.

Abstract

Achieving systemic tumor control across metastases is vital for long-term patient survival but remains intractable in many patients. High intrapatient heterogeneity persists, conferring many dissociated responses across metastatic lesions. Most studies of metastatic disease focus on tumor molecular and cellular features, which are crucial to elucidating the mechanisms underlying intrapatient heterogeneity. However, our understanding of intrapatient heterogeneity on the macroscopic level, such as lesion dynamics in growth, response, and relapse during treatment, remains rudimentary. This study investigated intrapatient heterogeneity through analyzing 116,542 observations of 40,612 lesions in 4,308 metastatic colorectal cancer (mCRC) patients. Despite significant differences in their response and relapse dynamics, metastatic lesions converged on four phenotypes that varied with anatomical site. Importantly, we found that organ-level relapse sequence was closely associated with patient survival, and that patients with the first relapses in the liver often had worse survival. In conclusion, our study provides insights into intrapatient response heterogeneity in mCRC and creates impetus for metastasis-specific therapeutics.

Introduction

Metastasis is the leading cause of cancer mortality[1]. Unfortunately, antitumor therapies are still designed mostly based on the biology of primary tumors, with little consideration of metastases[2,3]. Achieving systemic tumor control across metastases is critical for long-term survival but remains intractable in many patients. Some metastases respond highly to treatment while others do not at all, resulting in many dissociated and heterogeneous responses within patients[4–7]. Lesion-level response and relapse heterogeneity are common in many cancer types, but our understanding of such intrapatient heterogeneity and its relevance to prognosis remains rudimentary.

Most investigations of intrapatient lesion heterogeneity focus on tumor genetic mutations, clonal compositions, or transcriptomics [8–10]. These molecular and cellular characterizations are critical to elucidating the underlying mechanisms of intrapatient response heterogeneity[11,12]. However, it is equivalently critical to study intrapatient heterogeneity on the macroscopic level, such as distinct lesion dynamics in growth, response, and relapse during treatment, as well as their potential phenotypic convergence anatomically. These phenotypes would complement molecular and cellular analyses for a holistic view of intrapatient heterogeneity. This study sought to investigate intrapatient response heterogeneity through mapping lesion-specific response and relapse dynamics in metastatic CRC (mCRC).

Colorectal cancer (CRC) is the third leading cause of cancer-related death[13]. About 20% of CRC patients have distant metastases at diagnosis; the five-year relative survival rate is only 14% for these patients[14,15]. Intrapatient response heterogeneity is common in CRC patients treated with either standard chemotherapy alone or in combination with targeted therapy[16]. We, along with others, have found that high intrapatient response heterogeneity is associated with worse survival[16–19]. Importantly, we also found favorable responses in liver metastases predicted longer patient survival, compared to lesions in the lungs and lymph nodes (LN)[16]. Characterizing intrapatient response heterogeneity in mCRC is valuable for prognosis and therapies.

The local microenvironment selects tumor phenotypes in response to treatment, leading to heterogeneity across anatomically distinct lesions in terms of response and relapse dynamics[20,21]. Characterizing their phenotypic differences (divergence) or similarities (convergence) could yield insights into tumor ecological features and systemic resistance. To map the lesion-level response and relapse patterns in mCRC, we first applied a mathematical model to capture tumor growth dynamics in 4,308 mCRC patients. Next, individual lesion-specific response and relapse probabilities were mapped to predict their phenotypic divergence and convergence across anatomical sites. Last, we applied a machine learning approach to analyze the relapse sequence across lesions and its relevance to long-term patient survival. Our study provides insights into intrapatient phenotypic heterogeneity in mCRC and yields substantial implications for designing metastasis-specific therapeutics.

Results

Data Sources and Structure

To evaluate lesion-level response and relapse dynamics in mCRC, we collected longitudinal radiographical measurements of metastatic lesions in colorectal cancer (CRC) patients from Project Data Sphere. In total, 4,308 patients with 40,612 lesions from eight Phase III trials were included. The inclusion and exclusion criteria are presented in **Fig. 1a.** The distribution of lesion number across organs is shown in **Fig. 1b**. The total target lesions were 19,180 with 94,174 radiographic measurements, and there were 18,594 nontarget lesions and 2,838 new lesions with response status over time. Additional information including patients' demographic and clinical characteristics (e.g., age, gender, race, body mass index [BMI], tumor type, treatment history, RECIST response, and *KRAS* status), progression-free survival (PFS) and overall survival (OS) are reported in **Table 1**. We also included the tumor longitudinal measurements in a head and neck squamous cell carcinomas (mHNSCC) trial for external validation. The data was also from Project Data Sphere with similar criteria as CRC data (**Supplementary Fig. 3a**).

Model recapitulated tumor growth dynamics of individual lesions

The tumor growth dynamics of 19,180 target lesions with 94,174 radiographical measurements were recapitulated with a widely adopted growth model[22]. The three dynamic parameters in the model are the regression rate *Kd*, the fraction of non-responding cells *F*, and the progression rate *Kg* (**Fig. 2a).** The model was optimized using a nonlinear mixed effect (NLME) modeling approach, which allows the estimation of three dynamic parameters at the individual level and their inter-lesion variance in the population. Overall, the model adequately recapitulated the longitudinal profiles of tumor radiographic measurements for each lesion. The goodness-of-fit and model visual predictive check plots, as well as representative individual fittings, show good model predictive performance (**Supplementary Fig. 1**).

Population estimates and inter-lesion variances in tumor dynamic parameters are summarized in **Supplementary Table 1**. The parameters for individual lesions significantly differed across organs ($p < 0.0001$, **Fig. 2b**). Among all metastases, lesions in the bone exhibited the lowest response depth (1-*F*), while lesions in the genitourinary and reproductive (GR) system had the fastest progression rates (*Kg*), and kidney lesions showed the lowest regression rates (*Kd*). Among three most abundant metastatic sites (liver, lung, and LN), lesions in the liver showed the highest response depth but the fastest progression rates, suggesting the unique growth feature of liver lesions.

Higher treatment-resistant cell fraction *F* is associated with slower rates of regression (*Kd*, $r = -0.69$, $p < 0.005$) and faster rates of progression (*Kg*, $r = 0.53$, $p < 0.05$, **Fig. 2c**). Progression rates seemed to be independent of regression rates (**Fig. 2c**). Remarkably, no significant correlations were observed between baseline tumor burden and all tumor dynamic parameters (**Fig. 2d**). Large tumor burden, on the individual lesion level, did not necessarily confer slow regression rates, high treatment-resistant fractions, or slow progression rates, implying that tumor burden at baseline is not a robust prognostic factor in mCRC[23–25]. Notably, metastatic lesions under antibody targeted therapy (bevacizumab and/or panitumumab) plus chemotherapy (FOLFOX or FOLFIRI), compared to standard chemotherapy alone, showed significantly deeper response (effect size = 0.43) and lower progression rates (effect size = 0.26), but had a moderate effect on tumor regression rates (effect size = 0.06, **Supplementary Fig. 2**).

Response and relapse dynamics suggest phenotypic convergence on organ level

The tumor growth model predicted the longitudinal profiles of response and relapse for each target lesion. Response and relapse times were then derived as the duration from the start of treatment to the time of response or relapse per RECIST v1.1[26], respectively. We integrated the response time for both target and non-target lesions and the relapse time for all lesions, including the new ones, into random effect Cox proportional models[27]. The Cox model predicted the relative probabilities of lesion response or relapse at the organ level. Of note, treatment effects from either chemotherapy or combination therapy were included as a confounding factor in the Cox regression model. With that, we could focus on the organ-

intrinsic response and relapse characteristics. The hazard ratios for the response and relapse across organs are shown in **Fig. 3a** and **Fig. 3b**.

With abdominal lesions as the reference, metastatic lesions in the liver were most likely to respond to treatments, whereas lesions in the brain/central nervous system (CNS) were least likely (**Fig. 3a**). Lesions in the gastrointestinal (GI) system, skin, and bone were significantly less likely to respond than abdominal lesions. Lesions in the spleen, lung, and peritoneum showed comparable responses. The probability of relapse also differed greatly across anatomical sites (**Fig. 3b)**. The metastatic lesions with the highest likelihood of relapse were those in the brain/CNS, GR system, and liver, while lesions in the GI system, and regional and distal LNs were least likely.

We then integrated organ-specific response and relapse probabilities to investigate their potential phenotypic convergence across anatomical sites. As in **Fig. 3c**, an anatomical chart of organ-specific response and relapse probabilities was created based on their relative hazards in the Cox model. Four types of phenotypic features emerge in CRC-metastatic organs defined by their associated lesions' likelihood of response and relapse. Notably, bone and brain lesions had low response and high relapse probabilities (low-high phenotype), while liver lesions had high probabilities of both response and relapse (high-high phenotype). Patients with these metastases, particularly those with low-high phenotype, had much worse survival outcomes (OS median 378 days vs. 561 days, $p<0.0001$, **Supplementary Fig. 3a**). On the other side, metastatic lesions in the lung and LN showed high response and low relapse probabilities (high-low phenotypes). Patients who have metastases in high-low phenotype organs only tend to have a better prognosis than patients with other phenotypic metastases do (OS median 770 days vs. 524 days, $p<0.0001$, **Supplementary Fig. 3b**).

Interestingly, most metastatic lesions with high relapse probabilities tend to occur in organs known to have immunosuppressive microenvironments, such as the liver, bone, and brain/CNS[28–31]. To discern the influence of local tissue environment on tumor response phenotype, we performed the same analyses in head and neck squamous cell carcinomas (mHNSCC) to see whether a similar anatomical chart exists

(**Fig. 3d**). A total of 393 patients with 1,892 lesions were analyzed, including eleven metastatic organs (**Supplementary Fig. 4a** and **4b**). Patients' demographics are reported in **Supplementary Table 2**. The organ-specific hazard ratios for relapse and response were ranked, as we did in mCRC (**Supplementary Fig. 4c and 4d)**. In mHNSCC, metastases in the liver, bone, and brain also showed high relapse potential, in line with what we observed in mCRC. Metastatic lesions in the LNs exhibit a high-low phenotype, consistent with mCRC. Similar anatomical charts across cancer types suggest that organ-intrinsic microenvironmental factors, such as the local physical and immunological components, could be key modulators to the mechanisms underlying the probabilities of tumor response and relapse.

Treatment effects on organ-specific responses were also investigated. For simplicity, treatments were divided into two groups, chemotherapy alone and in combination with antibody targeted therapy. The combined antibody targeted therapies are either panitumumab or bevacizumab, or both. Surprisingly, combination with the antibody targeted therapies did not significantly influence organ-specific response probabilities (**Fig. 3e**), suggesting low direct cytotoxic effects of antibody-based therapies. Notably, the primary therapeutic benefit of antibody targeted therapies was to decrease relapse potential (**Fig. 3f**). Relapse hazards significantly decreased in most metastatic organs except for the skin, brain/CNS, spleen, and kidney. Taken together, antibody targeted therapies had the primary effect of decreasing lesion relapse probability but had limited influence on the lesion response probability. Interestingly, high-relapse organs in **Fig. 3c** also had high relapse probability during cytotoxic chemotherapies in **Fig. 3f**, suggesting a critical role for local tissue environments in long-term tumor control.

Relapse sequence across organs predicts patient survival

We built a k-means unsupervised clustering model to cluster patients based on their organ-level lesion relapse sequence to investigate their relevance to patient survival. Elbow sum of square[32] (**Supplementary Fig. 5a**) and Silhouette score[33] (**Supplementary Fig. 5b**) were calculated to determine the optimal k (= 5) in the final classification. Five groups of patients were identified with distinct patterns of organ-specific relapse sequences and were stratified by relapsing organ number and first-relapsing

organ: Mono-Organ (n=1,425), Hetero-Organ (n=801), Lung-First (n=577), Liver-First (n=1,194), and the Other-First (n=888) groups. The clinical demographics and baseline information of each group are summarized in **Supplementary Table 3**.

Organ-level relapse sequence is significantly correlated with long-term patient survival ($p < 0.0001$, **Fig. 4b**). As expected, patients with multiple organ relapses had worse survival than patients with only one organ relapse (OS median Hetero-Organ 385 days vs. Mono-Organ 653 days). Remarkably, despite comparable number of baseline metastases, patients whose first relapses were in the liver had a much worse prognosis than those whose first relapses were in lungs or other sites (OS median Liver-First 450 days vs. Lung-First 679 days vs. Other-First 581 days, **Fig. 4b**). This is consistent with earlier observations (**Fig. 3c)** that lesions in the lung had high-low phenotype that is often associated with good patient prognosis. Patients with relapse first in the liver had faster subsequent relapses than patients whose relapses occurred in lungs or other sites, suggesting that relapsing lesions in the liver have high systemic consequences ($p<0.0001$, **Fig. 4c**). It also aligns with our previous finding that the response of liver lesions to treatments strongly predicted patient survival[16].

Next, we performed k-means unsupervised clustering in the Hetero-Organ group to further investigate relapse patterns in patients with extensive metastases and relapses. Four groups of patients were optimally clustered (**Supplementary Fig. 5c and 5d**), and one distinctive feature among these clusters was the relapse order of liver lesions (**Supplementary Fig. 6a)**. Despite similar metastases, patients with first or second relapse occurring in the liver had worse survival than those with early relapses occurring in other organs (**Supplementary Fig. 6b and 6c**). This observation further underlines the importance of liver lesions to systemic response and resistance.

Targeted antibody therapies minimally influence lesion relapse sequence

We compared the relapse sequence in patients under different treatments (chemotherapy alone vs. combination with antibody targeted therapy). In patients with Liver-First, Lung-First or Other-First

relapse patterns, antibody targeted therapies significantly improved patient overall survival ($p < 0.0001$, **Fig. 5a**). However, neither the proportion of patients with each relapsing pattern (**Fig. 5b**) nor the sequence of relapse across metastatic organs were significantly different (**Fig. 5c-5e**). Relapses in the GR and pancreas occurred slightly earlier in antibody targeted therapy, which did not seem to translate meaningful difference in patient survival. Despite the similar sequence, patients under antibody targeted therapies had significantly slower first and second relapses, but had non-significant difference in the third or later relapses (**Fig. 5f-5g**). The average relapse times were much longer in combination therapy compared to chemotherapy alone.

In patients with the Hetero-Organ pattern, antibody targeted therapies did not meaningfully improve overall survival (**Supplementary Fig. 7a**) compared to chemotherapy alone, and the proportions of patients in each subcluster were similar between the two treatment groups (**Supplementary Fig. 7b**). Patients' relapse patterns and lesion relapse time were largely comparable, especially for those who had early liver lesion relapse (**Supplementary Fig. 7c-h**). Similarly, antibody targeted therapies did not influence lesion relapse sequence. Overall, the primary therapeutic benefit of antibody targeted therapies was to delay relapse in patients with few (< 4) metastatic organs, but not in those with broad metastases.

Machine learning model predicts lesion relapse sequence.

In order to predict patient relapse sequence at the time of diagnosis, we built a gradient boosting model using patient baseline characteristics and metastases profiles[34]. The model parameters are in **Supplementary Table 4**. The area under the receiver operating characteristic (ROC) curve of the testing data was 0.91, which indicated fair performance (**Supplementary Fig. 8a**). The model could predict Mono-Organ and Hetero-Organ groups better than Lung-First, Liver-First, and Other-First groups with higher area under the ROC curve. This indicates that more follow-up information is imperative to accurately predict the relapse sequences of the latter three groups (**Supplementary Fig. 8b**).

Discussion

Metastasis is responsible for the majority of cancer-related mortality. Unfortunately, systemic tumor control across metastases remains intractable in many patients. This study investigated inter-lesion heterogeneity by analyzing response dynamics of 40,612 lesions in 4,308 mCRC patients. Unlike most molecular characterizations of metastases, we focused on the phenotypic features associated with lesion response and relapse dynamics as well as the anatomical divergence and convergence of these features. Our analyses yielded several intriguing findings. First, metastases differed considerably in their response to treatment, with depth of response positively correlating with regression rate and negatively correlating with progression rate. Second, metastatic lesions within the same organ exhibited congruent response and relapse dynamics, converging upon four organ-level phenotypes. Metastatic lesions in the liver exhibited high response and high relapse probabilities (high-high phenotype), while lesions in the bone and brain/CNS had low response and high relapse probabilities (low-high phenotype). These phenotypes appear to be consistent across cancers. Third, we found that organ-level relapse sequence was closely associated with patient survival, and patients with the first relapse in the liver had worse survival outcomes compared to patients with first relapse in other sites.

This study quantified the degree of inter-lesion heterogeneity by modeling tumor regression and progression dynamics. By assuming first-order regression of drug-sensitive cancer cells (log-kill hypothesis), the empirical model adequately recapitulated the longitudinal size measurements on the lesion level. The first-order regression implies that drug-sensitive cancer cells may have only one rate-limiting step on the path to cell death[35]. Baseline tumor burden did not correlate with regression rates in our analyses, restating the first-order regression. Large tumors are often expected to have tumor regression potentially deviating from strict first-order kinetics because of their non-uniform drug distributions inside the tumor or only the surface tumor cells being actively proliferating and sensitive to treatment[36–38]. Our analyses did not find evidence to support these speculations. In contrast, despite large

sizes, metastatic lesions in the liver had relatively high regression rates compared to lesions at other organ sites.

The progression rates of drug-resistant tumor cells varied more between lesions than their associated regression rates and accounted the majority of intrapatient heterogeneity. Lesion relapse time was more closely associated with the progression rates than with the regression rates, in line with Stein et al., who reported that progression rates were a stronger predictor of patient survival[39]. If validated prospectively, the progression rates would offer more appropriate efficacy endpoints in clinical trials than the current ones that focus on the early response and regression, such as response rate and best of response.

Antibody therapies significantly increased response depths and decreased progression rates, but did not considerably affect regression rates. These observations indicate that the primary therapeutic benefit of combined antibody therapies is from growth suppression rather than direct cytotoxicity. In renal cell carcinomas, bevacizumab significantly reduced the growth rate constants, and the effect could become more apparent after relapse, in line with our observations in mCRC[40]. Interestingly, despite the broad evidence of its antibody-dependent cellular cytotoxicity (ADCC)[41] or complement-dependent cytotoxicity in vitro systems[42], the other antibody panitumumab in our analyses did not significantly affect tumor regression rates either, suggesting its low direct cytotoxicity in patients. In fact, the magnitude of the ADCC elicited by EGFR-targeting antibodies in patient remains hard to define, especially considering the restricted and highly varying infiltrations of effector cells in tumor beds[43,44]. Panitumumab (IgG2), compared to another EGFR-targeting antibody cetuximab (IgG1) showed reduced ADCC-dependent therapeutic effect, probably related to the reduced avidity of IgG2 for CD16, as compared to IgG1[45,46]. Unfortunately, our analyses did not include patients under cetuximab treatment, precluding direct comparison.

Metastatic lesions with lower fractions of resistant cells also had slower progression rates, suggesting consistent fitness of resistant cells before treatment and after relapse. However, metastatic lesions in the liver appear to behave differently; they had higher probability to respond, but also faster progression rates

than lesions in the LN and lungs, suggesting unique ecological properties of liver lesions. Our analyses highlight the importance of tissue microenvironments to metastatic phenotypes. Metastatic lesions with higher responses were typically found in the liver, spleen, LN, and lungs. These organs have discontinuous or fenestrated endothelial membranes, which may lead to higher drug exposure, potentially conferring high treatment responses[47,48]. In contrast, the organs bearing poorly-responding lesions are usually those with continuous endothelial membranes and thus more limited drug distribution, such as the muscle and brain/CNS[49–52]. Some organs that bear poorly-responding metastatic lesions, such as kidney and muscle, have relatively dense tissue matrices. This could limit the growth rate of metastatic lesions within these organs[53,54] and render them less responsive to cytotoxic chemotherapy[55,56].

On the other hand, organ-specific relapse probabilities seem to closely relate to the local immune microenvironments. Metastatic lesions with higher relapse potentials were found in the liver, bone, and brain/CNS, which either are immune-privileged or tolerogenic organs [20,21,28–31]. Interestingly, high relapses in these organs also occurred during cytotoxic chemotherapies that primarily work through DNA damage-induced cell death (**Fig. 3f**). Higher containment of tumor relapses in immunocompetent organs highlights the critical role anticancer immunity plays in long-term tumor control. Patients with highly relapsing lesions, such as lesions in the liver and bones, had much worse survival outcomes and likely require more effective and targeted therapeutics.

Tumor relapse is a serious impediment to cancer treatment, but organ-level relapse patterns remain poorly characterized. We found that early relapses in the liver, compared to early relapses in other sites, predicts worse patient survival and more rapid subsequent relapses. The liver's anatomical location, as a trafficking hub for CRC cells to spread to other organs, possibly underlies this finding[57]. By modeling large autopsy data sets in mCRC, Newton et al. highlighted that liver metastases could serve as tumor "spreaders" [58], and that there are multidirectional paths of tumor spread during progression[58,59]. Although we did not estimate transit probabilities from site to site, we speculate it is likely that early relapses in liver metastases could lead to more resistant cells spreading throughout the body and cause more frequent

subsequent relapses. Our population-level analysis supports this speculation and shows that liver metastases were often associated with a more pronounced tumor spread in the body.

The primary therapeutic benefit of antibody targeted therapies was to delay tumor progression and systemic relapses, without strong preferential effect on any organ-specific metastases. As such, antibody therapies did not affect relapse sequences, and the fraction of patients with the first relapse in the liver were largely comparable to chemotherapy alone. Unfortunately, in patients with multiple relapsed metastases (> 4 relapsed organs), the therapeutic benefit of antibody therapies is minimal, and more effective treatments remain sorely needed to treat patients with broad metastases.

In conclusion, we quantified intrapatient heterogeneity by modeling the longitudinal size measurement of metastatic lesions. This study provided a broad characterization of the phenotypic heterogeneity across metastatic lesions in mCRC, which could complement conventional molecular and cellular analyses to promote a more comprehensive view of intrapatient heterogeneity and yield substantial implications for metastasis-targeting therapies.

Methods

Data

Multiple mCRC and mHNSCC studies with longitudinal measurements of individual metastatic tumor information were included for the analyses. All datasets are accessible in Project Data Sphere (https://www.projectdatasphere.org/). Patients under one of the following conditions were excluded: (1) no target lesion longitudinal measurements; (2) baseline tumor size measured more than 12 weeks before the treatment. Patients' demographics and survival information were collected if applicable. The size and anatomical site about target/non-target lesion and occurring time and anatomical sites of new lesions were all recorded and analyzed if any.

All study protocols were approved by institutional review boards at each participating center. All patients have been provided written informed consent before study-related procedures were performed. All data sharing plans have been approved by the data sponsors.

Lesion-specific tumor growth dynamics

The longest diameter was converted to volume assuming the ellipsoidal shape of tumor (*Equation 1*) and the ratio of the tumor long versus short axis as 1.31[60]. An empirical tumor growth model (*Equation 2*) was used to recapitulate lesion-specific tumor growth dynamics.

$$V = \frac{(long\ axis)\times(short\ axis)^2}{2}$$ (*Equation 1*)

$$V = V0 \cdot [\, F \cdot e^{Kg \cdot t} + (1 - F) \cdot e^{-Kd \cdot t}]$$ (*Equation 2*)

V is the tumor volume, *V0* is the tumor baseline volume, *t* is the time. The model has three parameters for estimation: *F* is the fraction of non-responding tumor cells, with 1-*F* as the response depth; *Kg* is the progression rate and *Kd* is the regression rate. We fitted the model for all target lesions simultaneously using the Non-Linear Mixed Effect (NLME) method in Monolix2020R1. Stochastic approximation expectation-maximization (SAEM) algorithm was applied to search global optimum in the estimation. M3

method[61] was applied for quantifying size below the quantification of limit (< 200 mm^3)[62]. In the NLME method, the model parameters are described in *Equation 3-5*.

$$\ln(Kg^j) = \ln(\theta_{Kg}) + \eta_{Kg^j} \text{ (Equation 3)}$$

$$\ln(Kd^j) = \ln(\theta_{Kd}) + \eta_{Kd^j} \text{ (Equation 4)}$$

$$\text{logit}(F^j) = \text{logit}(\theta_F) + \eta_{F^j} \text{ (Equation 5)}$$

where θ is the population typical value, and η is the random effect with a log-normal distribution describing the difference between individuals and population average for each lesion *j*. Proportional error model was assumed. The initial values of *Kg*, *Kd* and *F* were 0.01 day^{-1}, 0.01 day^{-1}, and 0.1 (unitless).

Tumor response and relapse times

Tumor growth dynamic parameters were further taken to predict the longitudinal profiles of response and relapses for each target lesions. The longitudinal response and relapse status for each target or non-target lesion were determined per RECIST V1.1[26]. Target lesion response time (when the lesion size decreases ≥20% from baseline) and relapse time (when the lesion size increases ≥30% from tumor nadir or at least 200 mm^3 increase from nadir) were derived using tumor growth model with NLME-estimated parameters on the individual lesion level. Non-target lesions responded when "partial response" or "complete response" was firstly observed during the treatment and relapsed when "progressive disease" appeared in tumor evaluation. The relapse time for new lesions were defined as the detection time.

Cox proportional regression model

Cox proportional models were built to estimate lesion response and relapse probabilities across organs and treatments in R-4.1.0 and RStudio "coxme" package. Inter-patient variability was adjusted in the Cox models as random effect. Lesions without relapse or response during the treatment were labeled as censored by the last day of that patient in the trial. New lesions were considered only in the relapse hazard estimation.

Relapse pattern classification and prediction

We used the k-means machine learning algorithm to classify all the patients based on their organ relapse sequence in Spyder (Python 3.8) in Anaconda using the SCIKIT-LEARN 1.0.2 software package. Elbow method and Silhouette score were applied to find optimal k. The relapse patterns of patients clustered with different k were compared to help determine the choice of k in the final classification.

Gradient Boosting algorithm was applied to build a relapse pattern predictive model in Spyder (Python 3.8) in Anaconda using the SCIKIT-LEARN 1.0.2 software package. The research samples were randomly divided into a training and testing groups at a ratio of 4:1. The initial value of the hyperparameters used in this model was determined by parameter grid search, using 5-fold cross-validation and F1-score as a metric (**Supplementary Table 4**). The model outcome is the patient relapse sequence classified in k-means algorithm. Model predictors included patient clinical and demographic characteristics, as well as the baseline metastatic profiles, including the metastatic organs, metastatic numbers, metastatic target lesion baseline volume. Continuous predictors were normalized and categorical predictors were transformed to dummy variables. Performance index accuracy, precision, recall rate and area ROC curves were used to evaluate model performance.

Statistical analysis

Comparisons of continuous variables were performed using the two-tailed Mann–Whitney test or Kruskal–Wallis test. Multiple comparisons were adjusted by Dunn's test. PFS (defined as the start of therapies until RECIST-defined progression or death) and OS (defined as the start of therapies until patient death) among the groups were depicted using Kaplan–Meier curves and compared using log-rank tests. All the statistical tests were performed in GraphPad Prism 9.

References

1. Welch, D. R. & Hurst, D. R. Defining the hallmarks of metastasis. *Cancer Res.* **79**, 3011–3027 (2019).

2. Eccles, S. A. & Welch, D. R. Metastasis: recent discoveries and novel treatment strategies. *Lancet* **369**, 1742–1757 (2007).

3. Anderson, R. L. *et al.* A framework for the development of effective anti-metastatic agents. *Nat. Rev. Clin. Oncol.* **16**, 185–204 (2019).

4. Schmid, S. *et al.* Organ-specific response to nivolumab in patients with non-small cell lung cancer (NSCLC). *Cancer Immunol. Immunother.* **67**, 1825–1832 (2018).

5. Osorio, J. C. *et al.* Lesion-Level Response Dynamics to Programmed Cell Death Protein (PD-1) Blockade. *J. Clin. Oncol.* JCO1900709 (2019) doi:10.1200/JCO.19.00709.

6. Crusz, S. M. *et al.* Heterogeneous response and progression patterns reveal phenotypic heterogeneity of tyrosine kinase inhibitor response in metastatic renal cell carcinoma. *BMC Med.* **14**, 1–9 (2016).

7. Pires da Silva, I. *et al.* Site-specific response patterns, pseudoprogression, and acquired resistance in patients with melanoma treated with ipilimumab combined with anti–PD-1 therapy. *Cancer* **126**, 86–97 (2020).

8. Merz, M. *et al.* Deciphering spatial genomic heterogeneity at a single cell resolution in multiple myeloma. *Nat. Commun.* **13**, 1–15 (2022).

9. Wu, F. *et al.* Single-cell profiling of tumor heterogeneity and the microenvironment in advanced non-small cell lung cancer. *Nat. Commun.* **12**, 1–11 (2021).

10. Russo, M. *et al.* Tumor heterogeneity and lesion-specific response to targeted therapy in colorectal

cancer. *Cancer Discov.* **6**, 147–153 (2016).

11. Kashyap, A. *et al.* Quantification of tumor heterogeneity: from data acquisition to metric generation. *Trends Biotechnol.* (2021).

12. Huang, S. Reconciling non-genetic plasticity with somatic evolution in cancer. *Trends in cancer* **7**, 309–322 (2021).

13. Siegel, R. L. *et al.* Colorectal cancer statistics, 2020. *CA. Cancer J. Clin.* (2020).

14. Viale, P. H. The American Cancer Society's facts & figures: 2020 edition. *J. Adv. Pract. Oncol.* **11**, 135 (2020).

15. Biller, L. H. & Schrag, D. Diagnosis and treatment of metastatic colorectal cancer: a review. *Jama* **325**, 669–685 (2021).

16. Zhou, J., Li, Q. & Cao, Y. Spatiotemporal heterogeneity across metastases and organ-specific response informs drug efficacy and patient survival in colorectal cancer. *Cancer Res.* **81**, 2522–2533 (2021).

17. Asleh, K. *et al.* Proteomic analysis of archival breast cancer clinical specimens identifies biological subtypes with distinct survival outcomes. *Nat. Commun.* **13**, 1–19 (2022).

18. McDonald, K. A. *et al.* Tumor Heterogeneity Correlates with Less Immune Response and Worse Survival in Breast Cancer Patients. *Ann. Surg. Oncol.* **26**, 2191–2199 (2019).

19. Sveen, A. *et al.* Intra-patient inter-metastatic genetic heterogeneity in colorectal cancer as a key determinant of survival after curative liver resection. *PLoS Genet.* **12**, e1006225 (2016).

20. Binnewies, M. *et al.* Understanding the tumor immune microenvironment (TIME) for effective therapy. *Nat. Med.* **24**, 541–550 (2018).

21. Pao, W. *et al.* Tissue-specific immunoregulation: a call for better understanding of the

"immunostat" in the context of cancer. *Cancer Discov.* **8**, 395–402 (2018).

22. Wilkerson, J. *et al.* Estimation of tumour regression and growth rates during treatment in patients with advanced prostate cancer: a retrospective analysis. *Lancet Oncol.* **18**, 143–154 (2017).

23. Dai, W. *et al.* Does tumor size have its prognostic role in colorectal cancer? Re-evaluating its value in colorectal adenocarcinoma with different macroscopic growth pattern. *Int. J. Surg.* **45**, 105–112 (2017).

24. Kornprat, P. *et al.* Value of tumor size as a prognostic variable in colorectal cancer: a critical reappraisal. *Am. J. Clin. Oncol.* **34**, 43–49 (2011).

25. Santullo, F. *et al.* Tumor size as a prognostic factor in patients with stage IIa colon cancer. *Am. J. Surg.* **215**, 71–77 (2018).

26. Eisenhauer, E. A. *et al.* New response evaluation criteria in solid tumours: revised RECIST guideline (version 1.1). *Eur. J. Cancer* **45**, 228–247 (2009).

27. Murphy, S. A. Consistency in a proportional hazards model incorporating a random effect. *Ann. Stat.* **22**, 712–731 (1994).

28. Ilkovitch, D. & Lopez, D. M. The liver is a site for tumor-induced myeloid-derived suppressor cell accumulation and immunosuppression. *Cancer Res.* **69**, 5514–5521 (2009).

29. Mundy, G. R. Metastasis to bone: causes, consequences and therapeutic opportunities. *Nat. Rev. Cancer* **2**, 584–593 (2002).

30. Zhao, E. *et al.* Bone marrow and the control of immunity. *Cell. Mol. Immunol.* **9**, 11–19 (2012).

31. Fabry, Z., Schreiber, H. A., Harris, M. G. & Sandor, M. Sensing the microenvironment of the central nervous system: immune cells in the central nervous system and their pharmacological manipulation. *Curr. Opin. Pharmacol.* **8**, 496–507 (2008).

32. Syakur, M. A., Khotimah, B. K., Rochman, E. M. S. & Satoto, B. D. Integration k-means clustering method and elbow method for identification of the best customer profile cluster. in *IOP conference series: materials science and engineering* vol. 336 12017 (IOP Publishing, 2018).

33. Shahapure, K. R. & Nicholas, C. Cluster quality analysis using silhouette score. in *2020 IEEE 7th International Conference on Data Science and Advanced Analytics (DSAA)* 747–748 (IEEE, 2020).

34. Natekin, A. & Knoll, A. Gradient boosting machines, a tutorial. *Front. Neurorobot.* **7**, 21 (2013).

35. Yin, A., Moes, D. J. A. R., van Hasselt, J. G. C., Swen, J. J. & Guchelaar, H. A review of mathematical models for tumor dynamics and treatment resistance evolution of solid tumors. *CPT pharmacometrics Syst. Pharmacol.* **8**, 720–737 (2019).

36. Norton, L. The norton-simon hypothesis revisited. *Cancer Treat Rep* **70**, 163–169 (1986).

37. Fu, F., Nowak, M. A. & Bonhoeffer, S. Spatial heterogeneity in drug concentrations can facilitate the emergence of resistance to cancer therapy. *PLoS Comput. Biol.* **11**, e1004142 (2015).

38. Byrne, H. M. & Chaplain, M. A. J. Growth of necrotic tumors in the presence and absence of inhibitors. *Math. Biosci.* **135**, 187–216 (1996).

39. Stein, W. D. *et al.* Tumor regression and growth rates determined in five intramural NCI prostate cancer trials: the growth rate constant as an indicator of therapeutic efficacy. *Clin. Cancer Res.* **17**, 907–917 (2011).

40. Stein, W. D., Yang, J., Bates, S. E. & Fojo, T. Bevacizumab reduces the growth rate constants of renal carcinomas: a novel algorithm suggests early discontinuation of bevacizumab resulted in a lack of survival advantage. *Oncologist* **13**, 1055–1062 (2008).

41. Kurai, J. *et al.* Antibody-dependent cellular cytotoxicity mediated by cetuximab against lung cancer cell lines. *Clin. Cancer Res.* **13**, 1552–1561 (2007).

42. Bleeker, W. K. *et al.* Dual mode of action of a human anti-epidermal growth factor receptor monoclonal antibody for cancer therapy. *J. Immunol.* **173**, 4699–4707 (2004).

43. Weiner, L. M. Building better magic bullets—improving unconjugated monoclonal antibody therapy for cancer. *Nat. Rev. Cancer* **7**, 701–706 (2007).

44. Wheeler, D. L., Dunn, E. F. & Harari, P. M. Understanding resistance to EGFR inhibitors—impact on future treatment strategies. *Nat. Rev. Clin. Oncol.* **7**, 493–507 (2010).

45. Lee, S. C., Srivastava, R. M., López-Albaitero, A., Ferrone, S. & Ferris, R. L. Natural killer (NK): dendritic cell (DC) cross talk induced by therapeutic monoclonal antibody triggers tumor antigen-specific T cell immunity. *Immunol. Res.* **50**, 248–254 (2011).

46. Monteverde, M. *et al.* The relevance of ADCC for EGFR targeting: a review of the literature and a clinically-applicable method of assessment in patients. *Crit. Rev. Oncol. Hematol.* **95**, 179–190 (2015).

47. Claesson-Welsh, L., Dejana, E. & McDonald, D. M. Permeability of the endothelial barrier: identifying and reconciling controversies. *Trends Mol. Med.* **27**, 314–331 (2021).

48. Gifre-Renom, L., Daems, M., Luttun, A. & Jones, E. A. V. Organ-Specific Endothelial Cell Differentiation and Impact of Microenvironmental Cues on Endothelial Heterogeneity. *Int. J. Mol. Sci.* **23**, 1477 (2022).

49. Sarin, H. Physiologic upper limits of pore size of different blood capillary types and another perspective on the dual pore theory of microvascular permeability. *J. Angiogenes. Res.* **2**, 1–19 (2010).

50. Parton, R. G., Schrotz, P., Bucci, C. & Gruenberg, J. Plasticity of early endosomes. *J. Cell Sci.* **103**, 335–348 (1992).

51. Augustin, H. G., Kozian, D. H. & Johnson, R. C. Differentiation of endothelial cells: analysis of

the constitutive and activated endothelial cell phenotypes. *Bioessays* **16**, 901–906 (1994).

52. Cao, Y., Balthasar, J. P. & Jusko, W. J. Second-generation minimal physiologically-based pharmacokinetic model for monoclonal antibodies. *J. Pharmacokinet. Pharmacodyn.* **40**, 597–607 (2013).

53. Kay, K., Dolcy, K., Bies, R. & Shah, D. K. Estimation of solid tumor doubling times from progression-free survival plots using a novel statistical approach. *AAPS J.* **21**, 1–12 (2019).

54. Zharinov, G. M. *et al.* Prognostic value of tumor growth kinetic parameters in prostate cancer patients. *Oncotarget* **10**, 5020 (2019).

55. Lin, Z., Fan, Z., Zhang, X., Wan, J. & Liu, T. Cellular plasticity and drug resistance in sarcoma. *Life Sci.* **263**, 118589 (2020).

56. Amato, R. J. Chemotherapy for renal cell carcinoma. in *Seminars in oncology* vol. 27 177–186 (2000).

57. Clark, A. M., Ma, B., Taylor, D. L., Griffith, L. & Wells, A. Liver metastases: microenvironments and ex-vivo models. *Exp. Biol. Med.* **241**, 1639–1652 (2016).

58. Newton, P. K. *et al.* Spreaders and sponges define metastasis in lung cancer: a Markov chain Monte Carlo mathematical model. *Cancer Res.* **73**, 2760–2769 (2013).

59. Quinn, J. J. *et al.* Single-cell lineages reveal the rates, routes, and drivers of metastasis in cancer xenografts. *Science (80-.).* **371**, eabc1944 (2021).

60. Zhou, J., Liu, Y., Zhang, Y., Li, Q. & Cao, Y. Modeling tumor evolutionary dynamics to predict clinical outcomes for patients with metastatic colorectal cancer: a retrospective analysis. *Cancer Res.* **80**, 591–601 (2020).

61. Ahn, J. E., Karlsson, M. O., Dunne, A. & Ludden, T. M. Likelihood based approaches to handling

498 data below the quantification limit using NONMEM VI. *J. Pharmacokinet. Pharmacodyn.* **35**,
499 401–421 (2008).

500 62. Erdi, Y. E. Limits of tumor detectability in nuclear medicine and PET. *Mol. Imaging Radionucl.*
501 *Ther.* **21**, 23 (2012).

502

Data Availability

The clinical data that support the findings of this study are available in the Project Data Sphere, https://data.projectdatasphere.org/projectdatasphere/html/access. The machine learning algorithms codes were deposited at https://github.com/zhoujw14/Mapping-Metastasis.git. All source data for our model development and plotting will be provided upon request.

Acknowledgements

We thank Mr. Timothy Qi and Dr. Tyler Dunlap from University of North Carolina at Chapel Hill, Eshelman School of Pharmacy for providing valuable suggestions and edits for the manuscript.

Funding Source: National Institute of Health, R35GM119661

Author Contributions

Conceptualizations: J.Z., and Y.C.; methodology: J.Z., A.C., G.F., Q.L., and Y.C.; formal analysis: J.Z.; investigation: J.Z., Y.L., Q.L., and Y.C.; writing-original draft: J.Z., and Y.C.; writing-reviewing and editing: J.Z., A.C., G.F., Y.L., Q.L., and Y.C.; supervision: Y.C.

Competing Interests

All the authors declare no competing interests.

Correspondence and requests for materials should be addressed to Y.C.

519 **Tables**

520 **Table 1. Demographic information of colorectal cancer patients.**

Variable	
Age, years (mean, sd)	60.2 (10.8)
Gender (n, %)	
Male	2538 (58.9)
Female	1770 (41.1)
Race (n, %)	
White/Caucasian	3883 (90.1)
Black/African American	104 (2.4)
Asian	142 (3.3)
Other	179 (4.2)
Body Mass Index, kg/m^2 (mean, sd)	26.2 (5.1)
Tumor Type (n, %)	
Colon	2581 (59.9)
Rectal	1359 (31.5)
Unspecified	368 (8.5)
Prior Surgery (n, %)	
Yes	2993 (69.5)
No	1315 (30.5)
Prior Radiation (n, %)	
Yes	445 (10.3)
No	3345 (77.6)
Unknown	518 (12.1)

Treatment[1] (n, %)	
Bevacizumab plus chemotherapy	376 (8.7)
Bevacizumab plus FOLFOX	640 (14.9)
FOLFIRI alone	1303 (30.2)
FOLFOX alone	762 (17.7)
Panitumumab plus Bevacizumab plus chemotherapy	372 (8.6)
Panitumumab plus FOLFOX	441 (10.2)
Panitumumab plus FOLFIRI	424 (9.8)
Response (n, %)	
Complete Response	118 (2.7)
Partial Response	1473 (34.2)
Progressive Disease	781 (18.1)
Stable Disease	1806 (41.9)
Not Evaluable	130 (3)
Metastatic organ number (n, %)	
1	553 (12.8)
2	1159 (26.9)
3	1146 (26.6)
≥4	1450 (33.7)
KRAS status (n, %)	
Wild-Type	795 (18.4)
Mutant	593 (13.8)
Unknown	2920 (67.8)

[1]FOLFOX is the combination of folinic acid, fluorouracil and oxaliplatin. FOLFIRI is the combination of folinic acid, fluorouracil and irinotecan.

Figures

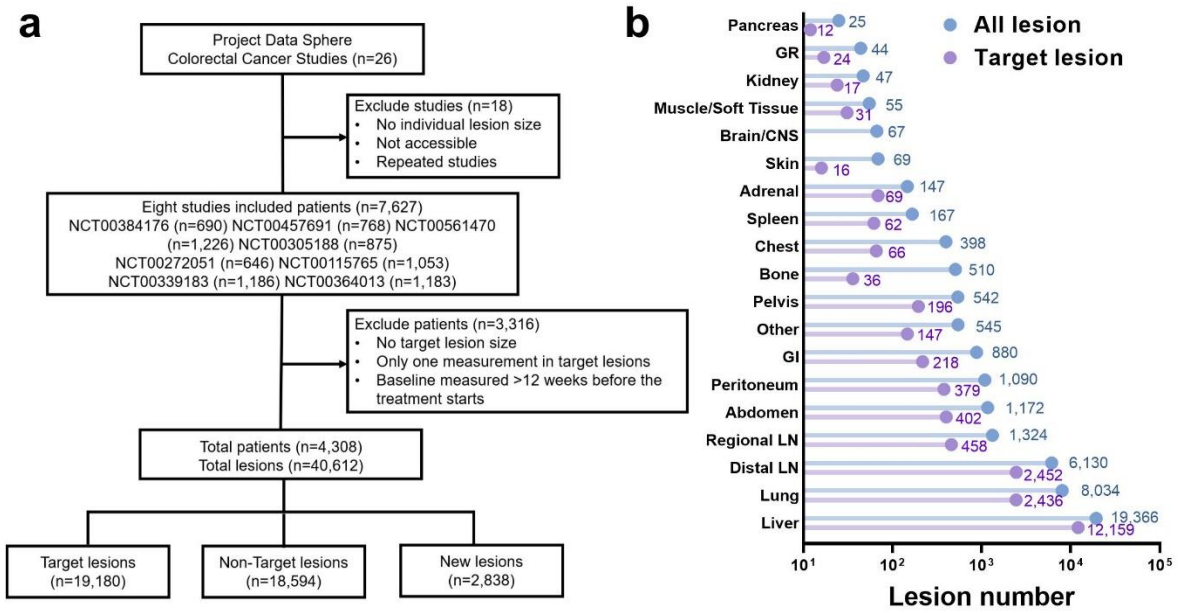

Fig. 1 Data source. a. CONSORT diagram of metastatic colorectal cancer data inclusion and exclusion criteria. **b.** The number of all lesions (target, non-target and new) and target lesions across organs. GR, Genitourinary and Reproductive; CNS, central nervous system; GI, Gastrointestinal tract; LN, lymph nodes.

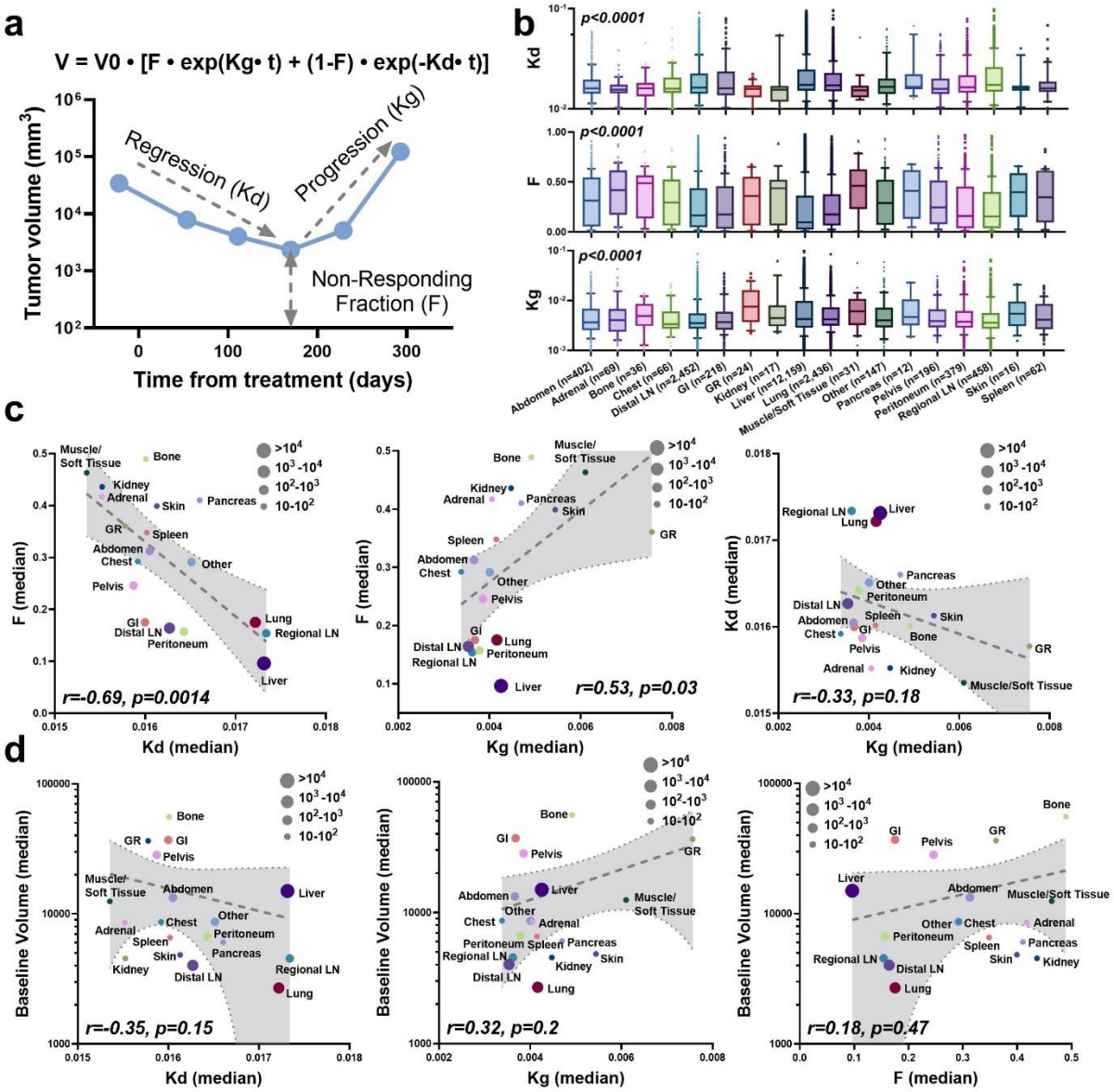

Fig. 2 Tumor response dynamics were recapitulated by modeling. a. Schematic plot of tumor growth model. **b.** Box plots of model parameters *Kd*, *F* and *Kg* across organs. Significance was calculated using Kruskal-Wallis tests. The box extends from the 25th to 75th percentiles and the line in the middle is plotted as the median. The whiskers are drawn down to the 10th percentile and up to the 90th percentile. Points below and above the whiskers represent individual lesions. **c.** The correlations between model parameters. **d.** The correlations between model parameters and tumor baseline volume. The size of the dots represents lesion number (reported in panel **b**). The dashed lines with gray area are the linear

regression with 95% confidence interval. The correlation coefficients and significance were calculated using two-tailed Pearson correlation tests.

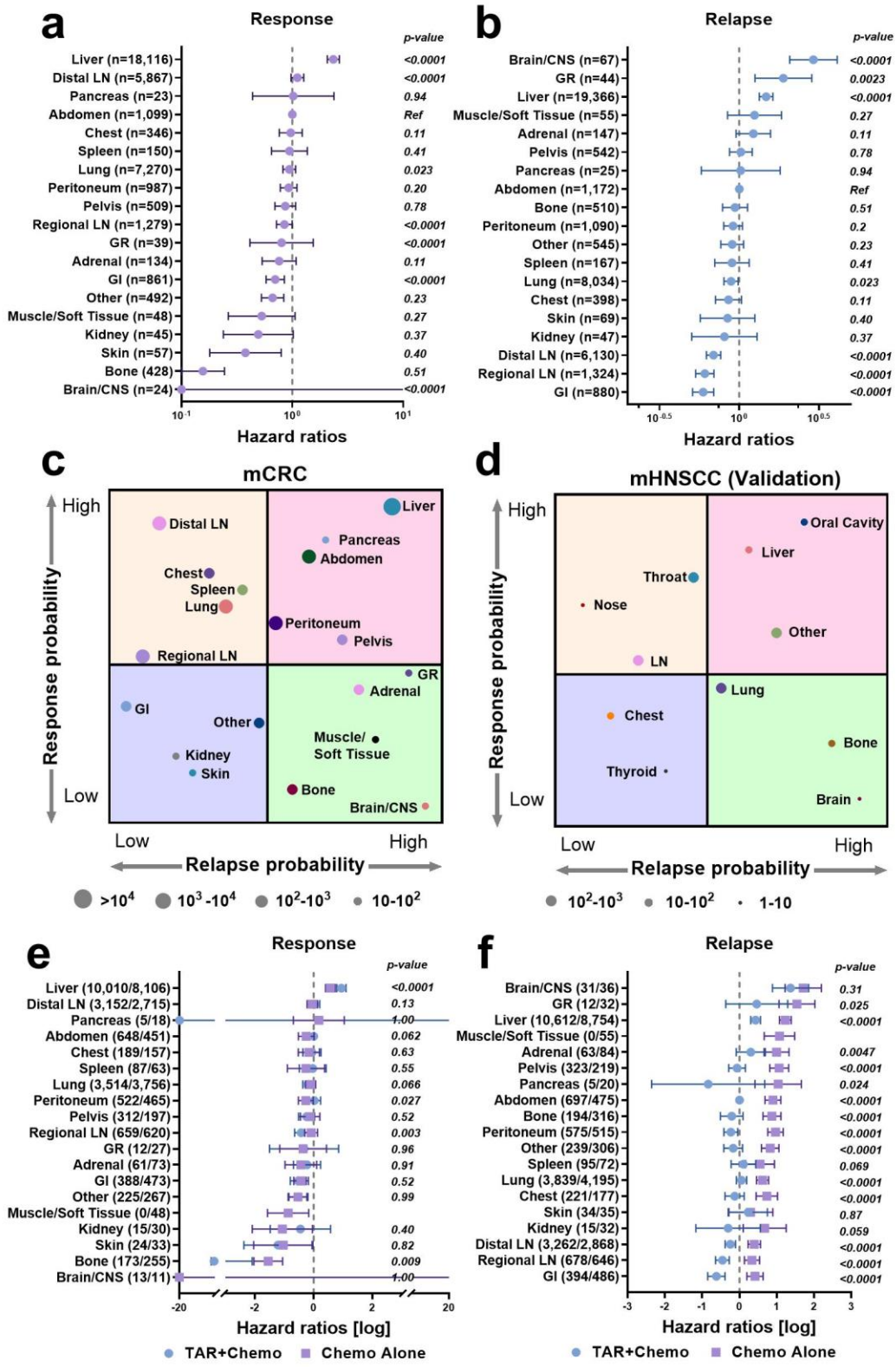
a
Response
p-value
Liver (n=18,116) <0.0001
Distal LN (n=5,867) <0.0001
Pancreas (n=23) 0.94
Abdomen (n=1,099) Ref
Chest (n=346) 0.11
Spleen (n=150) 0.41
Lung (n=7,270) 0.023
Peritoneum (n=987) 0.20
Pelvis (n=509) 0.78
Regional LN (n=1,279) <0.0001
GR (n=39) <0.0001
Adrenal (n=134) 0.11
GI (n=861) <0.0001
Other (n=492) 0.23
Muscle/Soft Tissue (n=48) 0.27
Kidney (n=45) 0.37
Skin (n=57) 0.40
Bone (428) 0.51
Brain/CNS (n=24) <0.0001
Hazard ratios
b
Relapse
p-value
Brain/CNS (n=67) <0.0001
GR (n=44) 0.0023
Liver (n=19,366) <0.0001
Muscle/Soft Tissue (n=55) 0.27
Adrenal (n=147) 0.11
Pelvis (n=542) 0.78
Pancreas (n=25) 0.94
Abdomen (n=1,172) Ref
Bone (n=510) 0.51
Peritoneum (n=1,090) 0.2
Other (n=545) 0.23
Spleen (n=167) 0.41
Lung (n=8,034) 0.023
Chest (n=398) 0.11
Skin (n=69) 0.40
Kidney (n=47) 0.37
Distal LN (n=6,130) <0.0001
Regional LN (n=1,324) <0.0001
GI (n=880) <0.0001
Hazard ratios
c
mCRC
High
Low
Response probability
Distal LN
Liver
Pancreas
Abdomen
Chest
Spleen
Lung
Peritoneum
Pelvis
Regional LN
GR
Adrenal
GI
Other
Muscle/
Soft Tissue
Kidney
Skin
Bone
Brain/CNS
Low
High
Relapse probability
>10^4
10^3 -10^4
10^2-10^3
10-10^2
d
mHNSCC (Validation)
High
Low
Response probability
Oral Cavity
Liver
Throat
Nose
Other
LN
Lung
Chest
Bone
Thyroid
Brain
Low
High
Relapse probability
10^2-10^3
10-10^2
1-10
e
Response
p-value
Liver (10,010/8,106) <0.0001
Distal LN (3,152/2,715) 0.13
Pancreas (5/18) 1.00
Abdomen (648/451) 0.062
Chest (189/157) 0.63
Spleen (87/63) 0.55
Lung (3,514/3,756) 0.066
Peritoneum (522/465) 0.027
Pelvis (312/197) 0.52
Regional LN (659/620) 0.003
GR (12/27) 0.96
Adrenal (61/73) 0.91
GI (388/473) 0.52
Other (225/267) 0.99
Muscle/Soft Tissue (0/48)
Kidney (15/30) 0.40
Skin (24/33) 0.82
Bone (173/255) 0.009
Brain/CNS (13/11) 1.00
Hazard ratios [log]
TAR+Chemo
Chemo Alone
f
Relapse
p-value
Brain/CNS (31/36) 0.31
GR (12/32) 0.025
Liver (10,612/8,754) <0.0001
Muscle/Soft Tissue (0/55)
Adrenal (63/84) 0.0047
Pelvis (323/219) <0.0001
Pancreas (5/20) 0.024
Abdomen (697/475) <0.0001
Bone (194/316) <0.0001
Peritoneum (575/515) <0.0001
Other (239/306) <0.0001
Spleen (95/72) 0.069
Lung (3,839/4,195) <0.0001
Chest (221/177) <0.0001
Skin (34/35) 0.87
Kidney (15/32) 0.059
Distal LN (3,262/2,868) <0.0001
Regional LN (678/646) <0.0001
GI (394/486) <0.0001
Hazard ratios [log]
TAR+Chemo
Chemo Alone

539

Fig. 3 Organ-level tumor response and relapse probabilities suggest phenotypic convergence. **a** and **b** rank the hazard ratio estimates with 95% confidence interval by organs on lesion response and relapse in colorectal cancer patients. **c** and **d** are the anatomical charts of organ-specific response and relapse hazard ratios in metastatic colorectal cancer (mCRC) and metastatic head and neck squamous cell carcinomas (mHNSCC). **e** and **f** are response and relapse hazard ratio with 95% confidence interval by organs stratified on treatments in mCRC. P-values were calculated by comparing the hazard ratios in antibody targeted therapies plus chemotherapy (TAR+Chemo) vs. chemotherapy alone (Chemo Alone) within each organ.

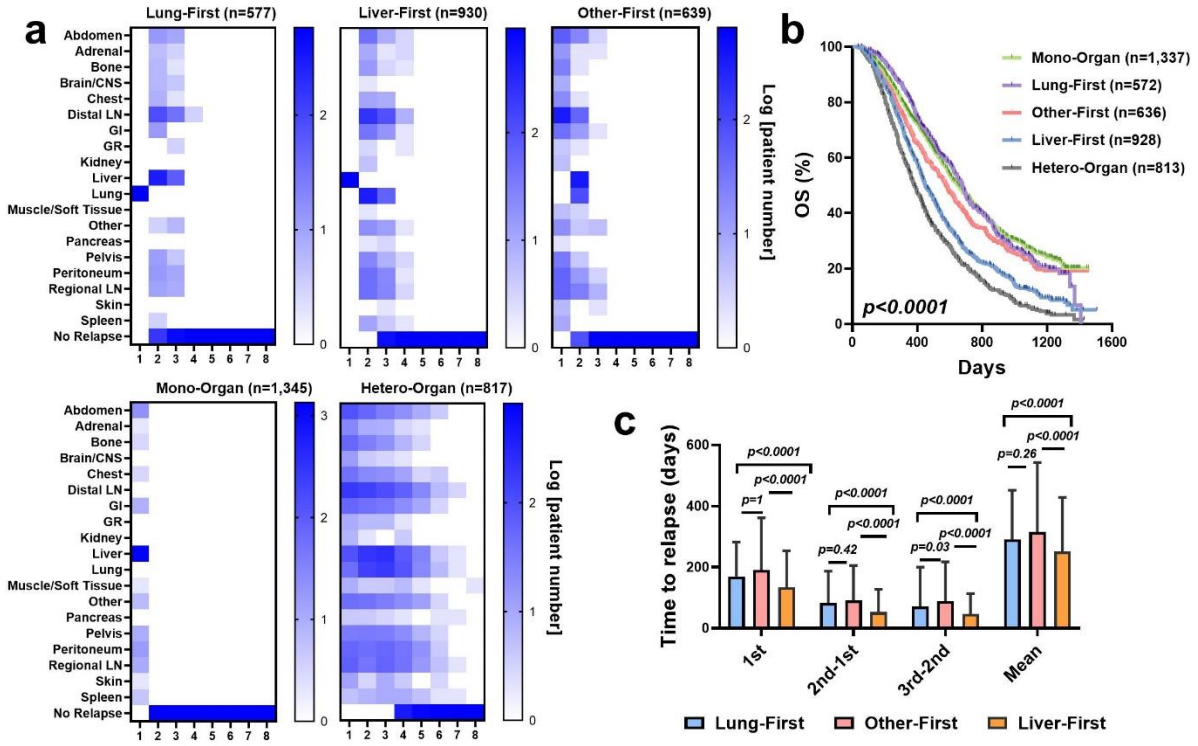

548

549 **Fig. 4 Patient relapse sequence association with patient survival. a.** Patients were clustered into five
550 groups based on their lesion relapse sequence. The column labels are the relapse sequence. Color of the
551 heatmap represents the log10 scale of patient number (all plus one to avoid zero values). **b.** Kaplan-Meier
552 curves of clustered patients overall survival. **c.** The mean and standard deviation of the first lesion relapse
553 time (1st), time between first and second relapse (2nd-1st), time between second and third relapse (3rd-
554 2nd), time between third and fourth relapse (4th-3rd), and the average relapse time in Lung-First (n=577),
555 Other-First (n=639), and Liver-First (n=930).

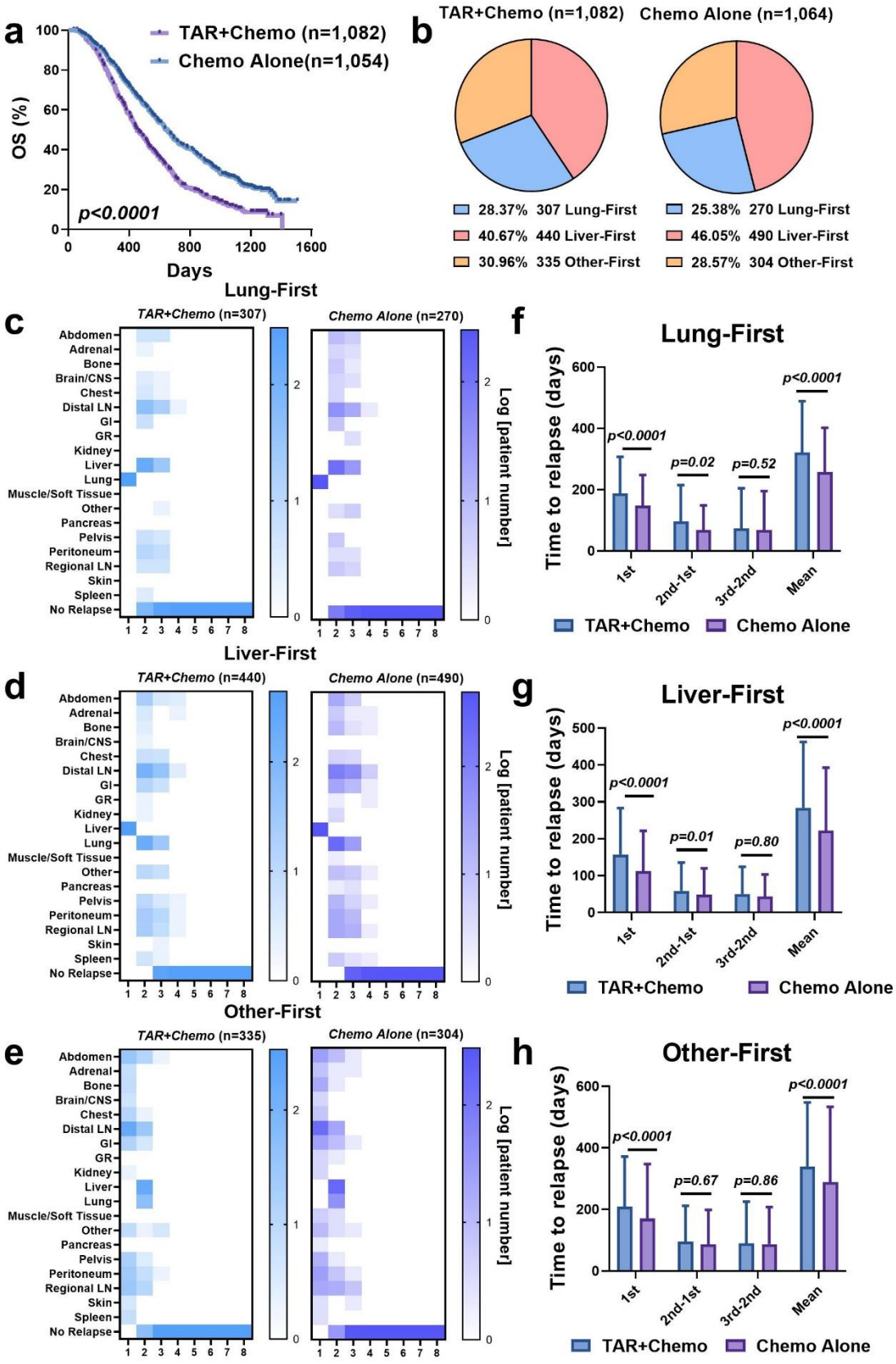
a
TAR+Chemo (n=1,082)
Chemo Alone(n=1,054)
OS (%)
p<0.0001
Days
b
TAR+Chemo (n=1,082)
Chemo Alone (n=1,064)
28.37% 307 Lung-First
40.67% 440 Liver-First
30.96% 335 Other-First
25.38% 270 Lung-First
46.05% 490 Liver-First
28.57% 304 Other-First
Lung-First
c
TAR+Chemo (n=307)
Chemo Alone (n=270)
Abdomen
Adrenal
Bone
Brain/CNS
Chest
Distal LN
GI
GR
Kidney
Liver
Lung
Muscle/Soft Tissue
Other
Pancreas
Pelvis
Peritoneum
Regional LN
Skin
Spleen
No Relapse
Log [patient number]
f
Lung-First
Time to relapse (days)
p<0.0001
p=0.02
p=0.52
p<0.0001
1st
2nd-1st
3rd-2nd
Mean
TAR+Chemo
Chemo Alone
Liver-First
d
TAR+Chemo (n=440)
Chemo Alone (n=490)
g
Liver-First
p<0.0001
p=0.01
p=0.80
p<0.0001
Other-First
e
TAR+Chemo (n=335)
Chemo Alone (n=304)
h
Other-First
p<0.0001
p=0.67
p=0.86
p<0.0001

556

Fig. 5. Targeted therapy decreases average time to relapse but has minimal effect on relapse sequence. a. Lung-First, Other-First and Liver-First patients overall survival stratified by treatments. **b.** Lung-First, Other-First and Liver-First patient proportions by treatments. **c, d,** and **e** are patient relapse sequences stratified by treatments. **f, g,** and **h** are the mean and standard deviation of the first lesion relapse time (1st), time between first and second relapse (2nd-1st), time between second and third relapse (3rd-2nd), time between third and fourth relapse (4th-3rd), and the average relapse time by treatments of the groups in **c, d,** and **e**. TAR+Chemo, antibody targeted therapies plus chemotherapy; Chemo Alone, chemotherapy alone.

Supplementary Files

This is a list of supplementary files associated with this preprint. Click to download.

- Supplementary3.13.pdf
- ClinicalTrialInformationNCOMMS2209853.xlsx